Direct numerical observation of real-space recollision in high-order harmonic generation from solids

Mrudul M. S.,[1] Adhip Pattanayak,[1] Misha Ivanov,[2,3,4,*] and Gopal Dixit[1,†]

[1]*Department of Physics, Indian Institute of Technology Bombay, Powai, Mumbai 400076, India*

[2]*Max-Born Institut, Max-Born Straße 2A, 12489 Berlin, Germany*

[3]*Blackett Laboratory, Imperial College London, London SW7 2AZ, United Kingdom*

[4]*Department of Physics, Humboldt University, Newtonstraße 15, 12489 Berlin, Germany*

(Received 15 November 2018; revised manuscript received 6 March 2019; published 28 October 2019)

The real-space picture of electron recollision with the parent ion guides our understanding of the highly nonlinear response of atoms and molecules to intense low-frequency laser fields. It is also an important player in high harmonic generation (HHG) in solids. It is typically viewed in the momentum space, as the recombination of the conduction band electron with the valence band hole, competing with another HHG mechanism, the strong-field driven Bloch oscillations. In this work, we use numerical simulations to directly test and confirm the real-space recollision picture as the key mechanism of HHG in solids. Our tests take advantage of the well-known characteristic features in the molecular harmonic spectra, associated with the real-space structure of the molecular ion. We show the emergence of analogous spectral features when similar real-space structures are present in the periodic potential of the solid-state lattice. This work demonstrates the capability of HHG imaging of spatial structures of a unit cell in solids.

DOI: 10.1103/PhysRevA.100.043420

I. INTRODUCTION

The importance of the simple physical picture [1–3] underlying high-harmonic generation (HHG) in atoms and molecules in strong laser fields can hardly be overstated. It plays a key role in using HHG to generate and control attosecond pulses [4–11]. It guides application of HHG as a time-resolved spectroscopic technique, linking the harmonic emission to the underlying electron-nuclear dynamics with attosecond temporal resolution [12–25]. These dynamics are mapped on all properties of the emitted light: amplitude, phase, and polarization [23,26].

The advent of intense midinfrared light sources triggered experiments on high-harmonic generation in solids, including dielectrics, semiconductors, nanostructures, and noble gas solids [27–39]. HHG in solids is attractive both as a possible compact source of XUV pulses [34,40,41] and as attosecond spectroscopy [42–47]. Spectroscopic applications include imaging energy bands [31,35], performing tomography of impurities in solids [48], and unraveling electron-hole dynamics at their intrinsic time scale [40,41,49,50], including phase transitions, both light driven and topological [42–46,51].

The dominant microscopic mechanism of HHG in solids is a topic of much debate, due in part to very different (from atoms and molecules) dependence on laser and material parameters [27,47,50,52–55]. One important mechanism is electron-hole recollision [56], leading to the (interband) electron-hole recombination (see, e.g., [33,52,57–60]). The second is the intraband current associated with laser driven Bloch oscillations (see, e.g., [30,34,61,62]).

Here we describe results of the numerical experiment which allows us to link directly HHG in solids with real-space electron-hole recollision. The key role of this mechanism, and the crucial importance of its real-space interpretation, has been highlighted in a beautiful recent paper [63]. We take advantage of the angstrom-scale spatial resolution embedded in the harmonic signal, well established in molecules [13,20,64–72]. The spatial information arises from half-scattering during electron-molecule recombination. It manifests in characteristic minima in the HHG spectra [64–66]. They are laser-intensity independent [13,64–66] and are associated with structure-based minima in the photorecombination cross sections [64–72], mirroring the well-known structure-related minima in photoionization. In diatomic molecules, the minima result from the Cohen-Fano interference of the two photoionization pathways originating at the two nuclei [73].

Clearly, if real-space recollision between the conduction-band electron and the valence-band hole underlies HHG in solids, it is supposed to exhibit the same Cohen-Fano–type interference minima when the unit cell of the periodic lattice potential has a two-center structure.

In dielectrics and wide-band-gap semiconductors, HHG is well described using semiconductor Bloch equations describing effective single-particle motion in the band-structure obtained, e.g., using density-functional theory methods or suitably chosen pseudopotentials. The quantitative accuracy of these methods has been well documented [33]. In our study, we restrict ourselves to wide band-gap materials, low-frequency drivers, and low excitation probability, where an effective single-particle description is adequate.

*Mikhail.Ivanov@mbi-berlin.de

†gdixit@phy.iitb.ac.in

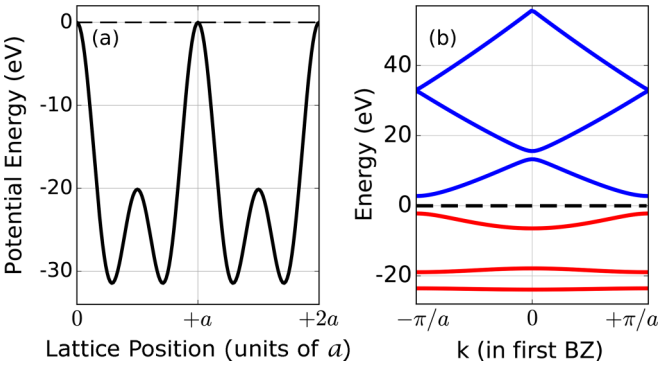

FIG. 1. The periodic bichromatic lattice potential [see Eq. (2)] (a) and the corresponding energy-band structure with valence (red) and conduction (blue) bands marked (b) within the first Brillouin zone.

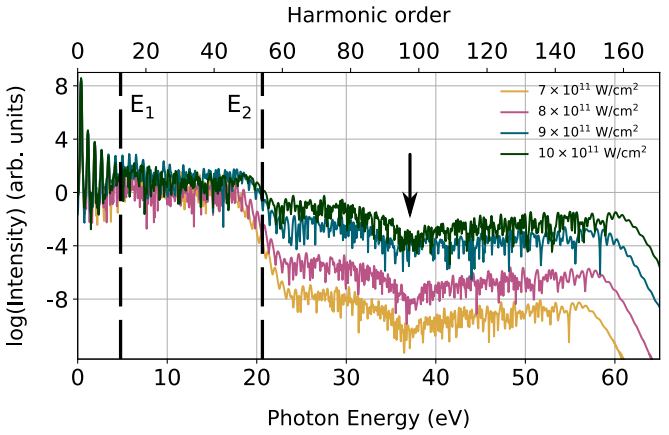

FIG. 2. High-harmonic spectrum as a function of driving laser intensity for the bichromatic lattice. Here, E_1 and E_2 mark the minimum (4.99 eV) and the maximum (19.67 eV) band gaps between the first conduction band and the valence band. The black arrow represents the position of the minimum. Grey-scale values of plots are chosen in the ascending order of the laser intensity.

II. THEORETICAL METHOD

To explore the idea, we model a semiconductor with a two-atom basis. In such a case, there will be two characteristic lengths for the unit cell: the interatomic distance as well as the lattice constant. When the laser polarization is along the direction of the interatomic bond, we can effectively model this system using a one-dimensional bichromatic lattice potential [see Fig. 1(a)]. The harmonic spectrum was obtained by solving the time-dependent Schroedinger equation (TDSE),

$$i\frac{\partial}{\partial t}|\Phi(t)\rangle = (\mathcal{H}_0 + \mathcal{H}_{\rm int})|\Phi(t)\rangle, \tag{1}$$

where $\mathcal{H}_0 = -\nabla^2/2 + V(x)$ is the field-free Hamiltonian, and $V(x)$ is the bichromatic lattice potential

$$V(x) = -V_0\left[(\alpha+\beta) - \alpha\cos\left(\frac{4\pi x}{a}\right) - \beta\cos\left(\frac{2\pi x}{a}\right)\right]. \tag{2}$$

Here, V_0 is the potential depth, a is the lattice constant. Atomic units are used throughout unless stated otherwise. Each unit cell has a double-well shape, with a the distance between the unit cells [Fig. 1(a)], and the ratio of α and β control the depth of the double-well potential. In the present study, $V_0 = 0.37$ a.u., $a = 8$ a.u., and $\alpha = \beta = 1$ are used. These values of V_0 and a are widely used to study HHG in solids [52,74–76]. Figure 1(b) shows the energy-band structure within the first Brillouin zone for this bichromatic lattice. The minimum-energy band gap is 4.99 eV at the edge of the Brillouin zone ($k = \pm\pi/a$).

To obtain the high-harmonic spectrum, we solve the TDSE in the velocity gauge within the Bloch-state basis [52,58], using the fourth-order Runge-Kutta method with 0.01 a.u. time step for the coupled differential equations as in Ref. [58]; no *ad hoc* dephasing is introduced.

Initially, all the valence bands are expected to be filled. Generally, one has to consider all crystal momentum states in the fully occupied valence bands, adding coherently the resulting laser-induced dipoles. However, excitation probabilities are low, and we found that including only those crystal momentum states that are located within 3% distance from the minimal band gap, in the highest valence band [third band in Fig. 1(b)], is sufficient to obtain the key spectral features of interest. Two other valence bands which are deeply bound are neglected in the calculation. The spectra were converged for the number of conduction bands. Similar approximations are used in Ref. [52]. To ensure the robustness of our findings, we have also simulated the HHG spectra by solving TDSE in real space. The results obtained from two different numerical approaches, in real space and in the Bloch state basis, show excellent agreement with each other [77]. The harmonic intensity is obtained from the time derivative of the time-dependent current as

$$I(\omega) = \left|\int dt \left(\frac{d}{dt}j(t)\right)e^{i\omega t}\right|^2. \tag{3}$$

Macroscopic propagation effects are not included.

III. RESULTS AND DISCUSSION

For the bichromatic lattice, the HHG spectrum is shown in Fig. 2, for an eight-optical-cycle linearly polarized laser pulse with a sine-square envelope and $\lambda = 3.2$ μm. Spectra corresponding to the four different laser intensities are shown: 7×10^{11} W/cm^2 (yellow), 8×10^{11} W/cm^2 (pink), 9×10^{11} W/cm^2 (blue), and 1×10^{12} W/cm^2 (green). The spectra exhibit both a primary and a secondary plateau and a sharp transition from the primary to the secondary plateau, with clear cutoffs. In the spectrum, E_1 and E_2 mark the minimum and the maximum band gaps between the first conduction band and the valence band.

The primary plateau arises due to the interband transition from the first conduction band to the valence band. The electron can also move to the higher conduction band via interband tunneling (see, e.g., [35,60,76]). Transitions from the higher-lying conduction band to the valence band lead to the secondary plateau (e.g., [35]). The intensity of the second plateau increases with the laser intensity, see Fig. 2, reflecting higher probability of the interband excitation to the higher conduction band. The harmonic cutoff in the second plateau

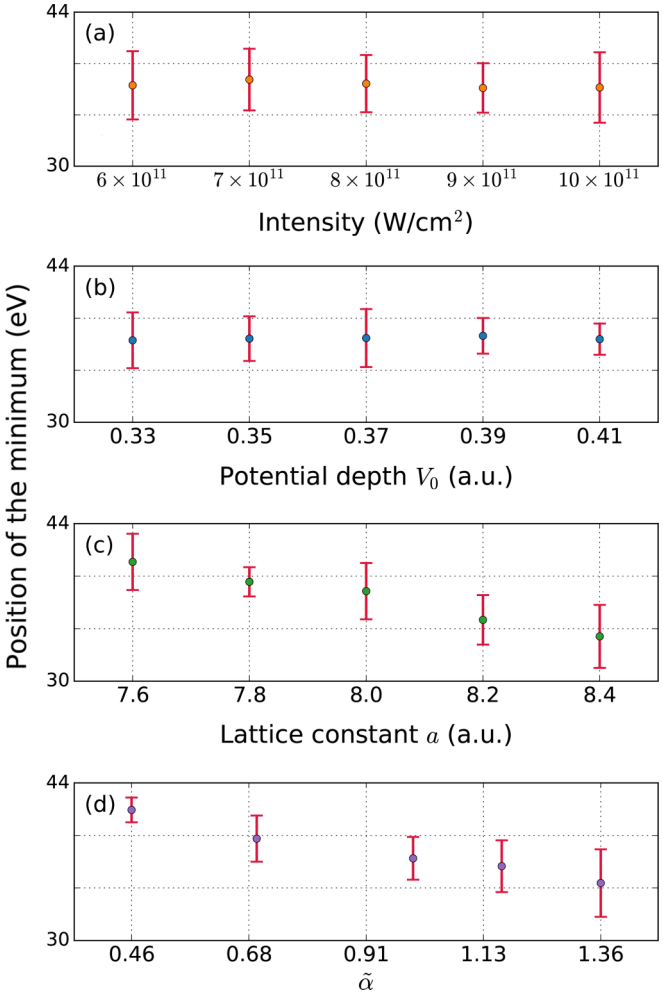

FIG. 3. The variation in the position of the minimum in the harmonic spectrum as a function of (a) intensity of the driving laser ($\lambda = 3.2$ μm, $V_0 = 0.37$ a.u., and $a = 8$ a.u.), (b) potential depth V_0 for the fixed lattice constant ($a = 8$ a.u.), (c) as a function of the lattice constant (a) (for $V_0 = 0.37$ a.u.), and (d) as a function of the depth of the double-well potential $\tilde{\alpha} = \alpha/\beta^2$ (for $V_0 = 0.37$ a.u., $a = 8$ a.u.). In (b)–(d), the laser intensity $I = 8 \times 10^{11}$ were used. The error bar represents the width of the interference minimum.

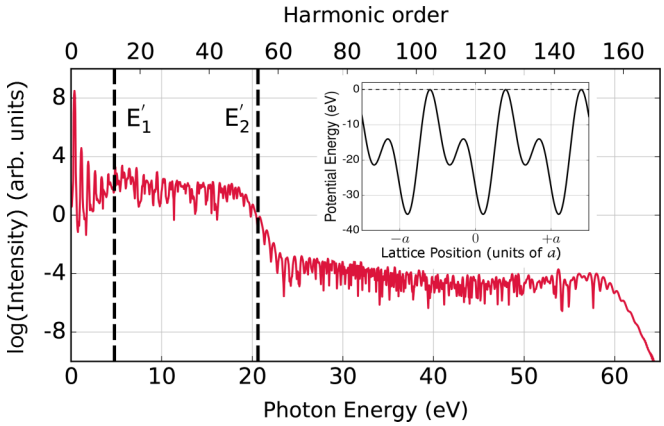

FIG. 4. High-harmonic spectrum for the asymmetric bichromatic periodic lattice (shown in inset). The harmonic spectrum is obtained for intensity of 8×10^{11} W/cm^2 and wavelength of 3.2 μm. Here, E_1' and E_2' mark the minimum (4.79 eV) and the maximum (20.63 eV) band gaps between the first conduction band and the valence band. The minimum-energy band gap is at the edge of the Brillouin zone ($k = \pm\pi/a$).

increases linearly with the field amplitude of driving laser, as is typical for solids [27,50,52,53].

The key feature of interest is the pronounced minimum in the second plateau, clearly present in Fig. 2 (see black arrow). To identify its physical origin, we plot the position of the minimum as a function of the laser intensity in Fig. 3(a). It shows that the position of the minimum is not sensitive to the laser intensity, just like the Cohen-Fano–type interference minimum in high-harmonic generation from molecules [64–70,78,79].

To verify this conclusion, we look at the position of the minimum as a function of the parameters of the bichromatic lattice potential [see Eq. (2)]. As expected for the Cohen-Fano–type interference in radiative recombination during recollision, the position of the minimum is independent of the depth of the bichromatic potential (V_0) as long as the distance between the wells does not change; see Fig. 3(b). However, the position of the minimum changes as soon as we start to vary the lattice constant a; see Fig. 3(c). As the lattice constant is increased, the minimum shifts towards lower photon energies, as it should. Identical observations have been reported for oriented molecules, where the interference minimum occurs at a lower harmonic order for larger internuclear bond length (or when the aligned molecular ensemble is rotated towards the field polarization) [64,65]. As can be seen from Eq. (2), the ratio of α and β controls the depth of the double-well potential. Changing this ratio changes the depth of the potential barrier between the two wells, and thus the distance between the two peaks of the corresponding wave function. For small $\tilde{\alpha} = \alpha/\beta^2$, the distance between the two peaks in the double-well wave function is smaller, and so the minimum is shifted to higher energies as is evident from Fig. 3(d). Note that the harmonic spectrum from the single color lattice (monochromatic lattice) does not exhibit any minimum in the spectrum (see also [52,74–76]). Therefore, analogous to structural minimum in oriented molecules, this minimum in solid HHG is related to the structure of the potential. It is important to note that the position of the minimum can be shifted to lower energies by changing different parameters of the lattice potential.

In diatomic molecules, the structural minimum associated with photorecombination disappears when the two nuclei are substantially different, so that the ground state is localized on a single nucleus. The same should happen here.

To check this effect, we introduce asymmetry into the double-well potential of the lattice as shown in Fig. 4 (inset). The asymmetry is introduced by adding a 90° phase difference between the two spatial frequency components of the lattice. The corresponding harmonic spectrum is shown in Fig. 4 for $I = 8 \times 10^{11}$ W/cm^2 and driving wavelength $\lambda = 3.2$ μm. While the overall harmonic spectrum is the same as for the symmetric bichromatic potential (see Figs. 2 and 4), the minimum disappears. Therefore, the minimum in solid HHG does indeed represent the structural minimum in recombination,

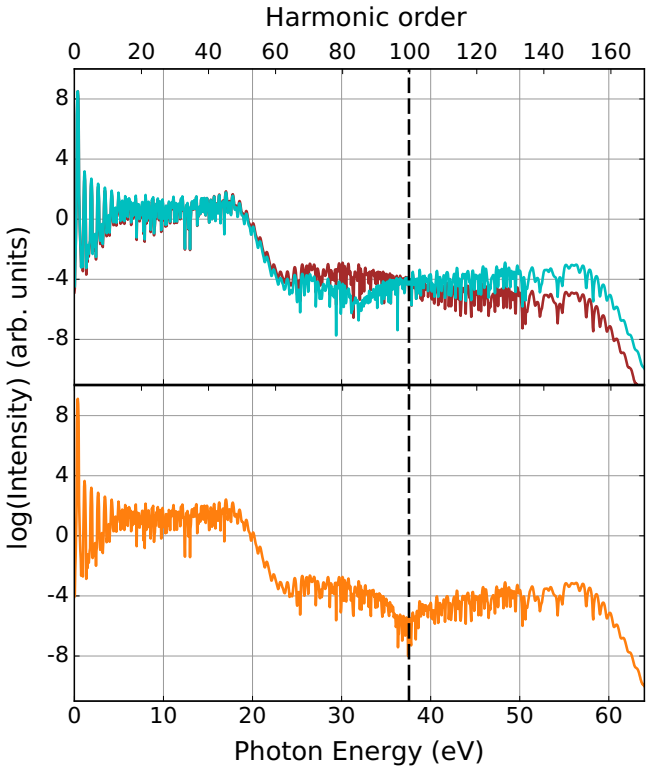

FIG. 5. Top: High-harmonic spectrum corresponding to the two components of Eq. (4): $-2\pi V_0/a[\langle\Phi(t)|\beta\sin(2\pi x/a)|\Phi(t)\rangle]$ (in brown or with higher grey-scale value) and $-2\pi V_0/a[\langle\Phi(t)|2\alpha\sin(4\pi x/a)|\Phi(t)\rangle]$ (in cyan or with lower grey-scale value). Bottom: The total high-harmonic spectrum corresponding to $\langle\Phi(t)|\nabla V|\Phi(t)\rangle$. The dotted line represents the region of the interference of the two components and resultant minimum in the total spectrum. The harmonic spectrum is obtained for intensity of 8×10^{11} W/cm^2 and wavelength of 3.2 μm.

in direct analogy with HHG in molecules, providing clear evidence of the recollision picture of HHG in solids.

Let us further explore the underlying mechanism responsible for the presence of minimum in a bichromatic lattice and its absence in the monochromatic (single color) lattice. In molecules, where such structural minimum is well studied, the total potential of the molecule and the bound-state wave function are written as a sum of two components located at the two nuclei. Consequently, the recombination amplitude also acquires two contributions, associated with the recombination onto each nucleus. Interference of these contributions leads to structural minima and maxima in photoionization and in molecular HHG spectra [64,65,69,70]. Note that while the exact position of the structural minimum is sensitive to the details of the wave function, the scattering potential, and possibly multielectron effects in photoionization or photorecombination, the presence of structure-induced features is completely general and is used to determine molecular structures.

The same arguments apply in our case. While the monochromatic lattice potential is a function of two reciprocal-lattice points $(0, 2\pi/a)$, the bichromatic potential is a function of three reciprocal-lattice points $(0, 2\pi/a, 4\pi/a)$. Let us write the dipole transition amplitude in the acceleration form as

$$\langle\Phi(t)|\nabla V|\Phi(t)\rangle = -\frac{2\pi V_0}{a}\left[\langle\Phi(t)|\beta\sin\left(\frac{2\pi x}{a}\right)|\Phi(t)\rangle + \langle\Phi(t)|2\alpha\sin\left(\frac{4\pi x}{a}\right)|\Phi(t)\rangle\right]. \quad (4)$$

The above equation shows that the dipole transition amplitude is a linear superposition of the two components, which are functions of the two different reciprocal-lattice points. The interference of these two terms produces the structural minimum in the harmonic spectrum of solids. We have calculated the harmonic spectrum from each of the two components as shown in Fig. 5. The first plateau of the two structures is matching while the second plateau behaves differently for the two components. The point at which the two contributions match in the second plateau can be identified as the position of the structural minimum. This also explains why there is no structural minimum in monochromatic lattice as there is no such two contributions to interfere. As it is clear from Eq. (4), only a and $\tilde{\alpha}$ are the parameters which make explicit changes in the two competing contributions differently, leading to a change in the position of the structural minima (see Fig. 4). Also, Eq. (4) shows that the dependence of V_0 appears in the prefactor. While the components of $|\Phi(t)\rangle$ carry the information about V_0, this does not lead to a considerable change in the position of the minimum for the energy range that we have considered. By adding a phase difference in the two interfering terms in Eq. (4), which is equivalent to creating an imbalance in the potential, we can modulate the interference as shown in Fig. 4.

IV. CONCLUSION

In this work, we have demonstrated that the real-space recollision picture passes an important numerical test, which makes a close analogy to the molecular picture. By providing direct numerical confirmation of the key role of recollision in coordinate space, our work also suggests that analysis of strong-field dynamics in solids can benefit from the real-space, as opposed to reciprocal space, perspective. This might be particularly interesting when the real-space electron excursion exceeds the size of the unit cell. Moreover, our work show that HHG from a solid has the potential to image the internal structures of a unit cell in solids.

ACKNOWLEDGMENTS

G.D. acknowledges a Ramanujan Fellowship (SB/S2/RJN-152/2015). M.I. acknowledges DFG QUTIF program, Grant No. IV 152/6-2 and from EPSRC/DSTL MURI Grant No. EP/N018680/1.

[1] P. B. Corkum, Phys. Rev. Lett. **71**, 1994 (1993).

[2] M. Lewenstein, P. Balcou, M. Y. Ivanov, A. L'Huillier, and P. B. Corkum, Phys. Rev. A **49**, 2117 (1994).

[3] K. J. Schafer, B. Yang, L. F. DiMauro, and K. C. Kulander, Phys. Rev. Lett. **70**, 1599 (1993).

[4] P. M. Paul, E. S. Toma, P. Breger, G. Mullot, F. Augé, P. Balcou, H. G. Muller, and P. Agostini, Science **292**, 1689 (2001).

[5] G. Sansone, E. Benedetti, F. Calegari, C. Vozzi, L. Avaldi, R. Flammini, L. Poletto, P. Villoresi, C. Altucci, R. Velotta *et al.*, Science **314**, 443 (2006).

[6] T. Popmintchev, M. C. Chen, D. Popmintchev, P. Arpin, S. Brown, S. Ališauskas, G. Andriukaitis, T. Balčiunas, O. D. Mücke, A. Pugzlys *et al.*, Science **336**, 1287 (2012).

[7] E. Goulielmakis, M. Schultze, M. Hofstetter, V. S. Yakovlev, J. Gagnon, M. Uiberacker, A. L. Aquila, E. M. Gullikson, D. T. Attwood, R. Kienberger *et al.*, Science **320**, 1614 (2008).

[8] K. T. Kim, C. Zhang, T. Ruchon, J. F. Hergott, T. Auguste, D. M. Villeneuve, P. B. Corkum, and F. Quéré, Nat. Photon. **7**, 651 (2013).

[9] J. Li, X. Ren, Y. Yin, K. Zhao, A. Chew, Y. Cheng, E. Cunningham, Y. Wang, S. Hu, Y. Wu *et al.*, Nat. Commun. **8**, 186 (2017).

[10] F. Silva, S. M. Teichmann, S. L. Cousin, M. Hemmer, and J. Biegert, Nat. Commun. **6**, 6611 (2015).

[11] T. Gaumnitz, A. Jain, Y. Pertot, M. Huppert, I. Jordan, F. Ardana-Lamas, and H. J. Wörner, Opt. Express **25**, 27506 (2017).

[12] F. Krausz and M. Ivanov, Rev. Mod. Phys. **81**, 163 (2009).

[13] O. Smirnova, Y. Mairesse, S. Patchkovskii, N. Dudovich, D. Villeneuve, P. Corkum, and M. Ivanov, Nature (London) **460**, 972 (2009).

[14] G. Dixit, O. Vendrell, and R. Santra, Proc. Natl. Acad. Sci. USA **109**, 11636 (2012).

[15] T. Bredtmann, M. Ivanov, and G. Dixit, Nat. Commun. **5**, 5589 (2014).

[16] P. H. Bucksbaum, Science **317**, 766 (2007).

[17] P. B. Corkum and F. Krausz, Nat. Phys. **3**, 381 (2007).

[18] F. Lépine, M. Y. Ivanov, and M. J. J. Vrakking, Nat. Photon. **8**, 195 (2014).

[19] S. Baker, J. S. Robinson, C. A. Haworth, H. Teng, R. A. Smith, C. C. Chirilă, M. Lein, J. W. G. Tisch, and J. P. Marangos, Science **312**, 424 (2006).

[20] S. Haessler, J. Caillat, W. Boutu, C. Giovanetti-Teixeira, T. Ruchon, T. Auguste, Z. Diveki, P. Breger, A. Maquet, B. Carré *et al.*, Nat. Phys. **6**, 200 (2010).

[21] R. E. F. Silva, F. Catoire, P. Rivière, H. Bachau, and F. Martín, Phys. Rev. Lett. **110**, 113001 (2013).

[22] B. D. Bruner, Z. Mašín, M. Negro, F. Morales, D. Brambila, M. Devetta, D. Faccialà, A. G. Harvey, M. Ivanov, Y. Mairesse *et al.*, Faraday Discuss. **194**, 369 (2016).

[23] O. Smirnova, S. Patchkovskii, Y. Mairesse, N. Dudovich, D. Villeneuve, P. Corkum, and M. Y. Ivanov, Phys. Rev. Lett. **102**, 063601 (2009).

[24] X. B. Bian and A. D. Bandrauk, Phys. Rev. Lett. **105**, 093903 (2010).

[25] T. Morishita, A.-T. Le, Z. Chen, and C. D. Lin, Phys. Rev. Lett. **100**, 013903 (2008).

[26] O. Raz, O. Schwartz, D. Austin, A. S. Wyatt, A. Schiavi, O. Smirnova, B. Nadler, I. A. Walmsley, D. Oron, and N. Dudovich, Phys. Rev. Lett. **107**, 133902 (2011).

[27] S. Ghimire, A. D. DiChiara, E. Sistrunk, P. Agostini, L. F. DiMauro, and D. A. Reis, Nat. Phys. **7**, 138 (2011).

[28] S. Ghimire, A. D. DiChiara, E. Sistrunk, U. B. Szafruga, P. Agostini, L. F. DiMauro, and D. A. Reis, Phys. Rev. Lett. **107**, 167407 (2011).

[29] B. Zaks, R. B. Liu, and M. S. Sherwin, Nature (London) **483**, 580 (2012).

[30] O. Schubert, M. Hohenleutner, F. Langer, B. Urbanek, C. Lange, U. Huttner, D. Golde, T. Meier, M. Kira, S. W. Koch *et al.*, Nat. Photon. **8**, 119 (2014).

[31] G. Vampa, T. J. Hammond, N. Thiré, B. E. Schmidt, F. Légaré, C. R. McDonald, T. Brabec, D. D. Klug, and P. B. Corkum, Phys. Rev. Lett. **115**, 193603 (2015).

[32] G. Vampa, T. J. Hammond, N. Thiré, B. E. Schmidt, F. Légaré, C. R. McDonald, T. Brabec, and P. B. Corkum, Nature (London) **522**, 462 (2015).

[33] M. Hohenleutner, F. Langer, O. Schubert, M. Knorr, U. Huttner, S. W. Koch, M. Kira, and R. Huber, Nature (London) **523**, 572 (2015).

[34] T. T. Luu, M. Garg, S. Y. Kruchinin, A. Moulet, M. T. Hassan, and E. Goulielmakis, Nature (London) **521**, 498 (2015).

[35] G. Ndabashimiye, S. Ghimire, M. Wu, D. A. Browne, K. J. Schafer, M. B. Gaarde, and D. A. Reis, Nature (London) **534**, 520 (2016).

[36] Y. S. You, Y. Yin, Y. Wu, A. Chew, X. Ren, F. Zhuang, S. Gholam-Mirzaei, M. Chini, Z. Chang, and S. Ghimire, Nat. Commun. **8**, 724 (2017).

[37] A. A. Lanin, E. A. Stepanov, A. B. Fedotov, and A. M. Zheltikov, Optica **4**, 516 (2017).

[38] M. Sivis, M. Taucer, G. Vampa, K. Johnston, A. Staudte, A. Y. Naumov, D. M. Villeneuve, C. Ropers, and P. B. Corkum, Science **357**, 303 (2017).

[39] F. Langer, C. P. Schmid, S. Schlauderer, M. Gmitra, J. Fabian, P. Nagler, C. Schüller, T. Korn, P. G. Hawkins, J. T. Steiner *et al.*, Nature (London) **557**, 76 (2018).

[40] G. Vampa and T. Brabec, J. Phys. B **50**, 083001 (2017).

[41] S. Y. Kruchinin, F. Krausz, and V. S. Yakovlev, Rev. Mod. Phys. **90**, 021002 (2018).

[42] R. E. F. Silva, I. V. Blinov, A. N. Rubtsov, O. Smirnova, and M. Ivanov, Nat. Photon. **12**, 266 (2018).

[43] R. E. F. Silva, Á. Jiménez-Galán, B. Amorim, O. Smirnova, and M. Ivanov, Nat. Photon. (2019), doi:10.1038/s41566-019-0516-1.

[44] D. Bauer and K. K. Hansen, Phys. Rev. Lett. **120**, 177401 (2018).

[45] A. Chacón, W. Zhu, S. P. Kelly, A. Dauphin, E. Pisanty, A. Picón, C. Ticknor, M. F. Ciappina, A. Saxena, and M. Lewenstein, arXiv:1807.01616.

[46] J. Reimann, S. Schlauderer, C. P. Schmid, F. Langer, S. Baierl, K. A. Kokh, O. E. Tereshchenko, A. Kimura, C. Lange, J. Güdde *et al.*, Nature **562**, 396 (2018).

[47] I. Floss, C. Lemell, G. Wachter, V. Smejkal, S. A. Sato, X. M. Tong, K. Yabana, and J. Burgdörfer, Phys. Rev. A **97**, 011401(R) (2018).

[48] S. Almalki, A. M. Parks, G. Bart, P. B. Corkum, T. Brabec, and C. R. McDonald, Phys. Rev. B **98**, 144307 (2018).

[49] T. Higuchi, M. I. Stockman, and P. Hommelhoff, Phys. Rev. Lett. **113**, 213901 (2014).

[50] S. Ghimire, G. Ndabashimiye, A. D. DiChiara, E. Sistrunk, M. I. Stockman, P. Agostini, L. F. DiMauro, and D. A. Reis, J. Phys. B **47**, 204030 (2014).

[51] Y. Murakami, M. Eckstein, and P. Werner, Phys. Rev. Lett. **121**, 057405 (2018).
[52] M. Wu, S. Ghimire, D. A. Reis, K. J. Schafer, and M. B. Gaarde, Phys. Rev. A **91**, 043839 (2015).
[53] T.-Y. Du and X.-B. Bian, Opt. Express **25**, 151 (2017).
[54] N. Tancogne-Dejean, O. D. Mücke, F. X. Kärtner, and A. Rubio, Phys. Rev. Lett. **118**, 087403 (2017).
[55] N. Tancogne-Dejean, O. D. Mücke, F. X. Kärtner, and A. Rubio, Nat. Commun. **8**, 745 (2017).
[56] G. Vampa, C. R. McDonald, G. Orlando, D. D. Klug, P. B. Corkum, and T. Brabec, Phys. Rev. Lett. **113**, 073901 (2014).
[57] C. R. McDonald, G. Vampa, P. B. Corkum, and T. Brabec, Phys. Rev. A **92**, 033845 (2015).
[58] M. Korbman, S. Y. Kruchinin, and V. S. Yakovlev, New J. Phys. **15**, 013006 (2013).
[59] G. Vampa, C. R. McDonald, G. Orlando, P. B. Corkum, and T. Brabec, Phys. Rev. B **91**, 064302 (2015).
[60] P. G. Hawkins, M. Y. Ivanov, and V. S. Yakovlev, Phys. Rev. A **91**, 013405 (2015).
[61] P. G. Hawkins and M. Y. Ivanov, Phys. Rev. A **87**, 063842 (2013).
[62] S. Ghimire, A. D. DiChiara, E. Sistrunk, G. Ndabashimiye, U. B. Szafruga, A. Mohammad, P. Agostini, L. F. DiMauro, and D. A. Reis, Phys. Rev. A **85**, 043836 (2012).
[63] Y. S. You, E. Cunningham, D. A. Reis, and S. Ghimire, J. Phys. B **51**, 114002 (2018).
[64] M. Lein, N. Hay, R. Velotta, J. P. Marangos, and P. L. Knight, Phys. Rev. Lett. **88**, 183903 (2002).
[65] M. Lein, N. Hay, R. Velotta, J. P. Marangos, and P. L. Knight, Phys. Rev. A **66**, 023805 (2002).
[66] M. Lein, J. Phys. B **40**, R135 (2007).
[67] C. Vozzi, F. Calegari, E. Benedetti, J. P. Caumes, G. Sansone, S. Stagira, M. Nisoli, R. Torres, E. Heesel, N. Kajumba *et al.*, Phys. Rev. Lett. **95**, 153902 (2005).
[68] T. Kanai, S. Minemoto, and H. Sakai, Nature (London) **435**, 470 (2005).
[69] S. Odžak and D. B. Milošević, Phys. Rev. A **79**, 023414 (2009).
[70] R. Torres, T. Siegel, L. Brugnera, I. Procino, J. G. Underwood, C. Altucci, R. Velotta, E. Springate, C. Froud, I. C. E. Turcu, S. Patchkovskii, M. Y. Ivanov, O. Smirnova, and J. P. Marangos, Phys. Rev. A **81**, 051802(R) (2010).
[71] S. Sukiasyan, S. Patchkovskii, O. Smirnova, T. Brabec, and M. Y. Ivanov, Phys. Rev. A **82**, 043414 (2010).
[72] K.-J. Yuan, X.-B. Bian, and A. D. Bandrauk, Phys. Rev. A **90**, 023407 (2014).
[73] H. D. Cohen and U. Fano, Phys. Rev. **150**, 30 (1966).
[74] X. Liu, X. Zhu, X. Zhang, D. Wang, P. Lan, and P. Lu, Opt. Express **25**, 29216 (2017).
[75] X. Liu, X. Zhu, P. Lan, X. Zhang, D. Wang, Q. Zhang, and P. Lu, Phys. Rev. A **95**, 063419 (2017).
[76] T. Ikemachi, Y. Shinohara, T. Sato, J. Yumoto, M. Kuwata-Gonokami, and K. L. Ishikawa, Phys. Rev. A **95**, 043416 (2017).
[77] To be published elsewhere.
[78] W. Boutu, S. Haessler, H. Merdji, P. Breger, G. Waters, M. Stankiewicz, L. J. Frasinski, R. Taieb, J. Caillat, A. Maquet *et al.*, Nat. Phys. **4**, 545 (2008).
[79] X. Zhou, R. Lock, W. Li, N. Wagner, M. M. Murnane, and H. C. Kapteyn, Phys. Rev. Lett. **100**, 073902 (2008).